Proceedings of ASME Turbo Expo 2012
GT2012
June 11-15, 2012, Copenhagen, Denmark

GT2012-69138

LIFE PREDICTION FEASIBILITY IN TMF VIA STRESS/STRAIN DATA FROM A VISCOPLASTICITY-BASED NUMERICAL MODEL

Justin Karl
University of Central Florida
Orlando, FL, USA
jkarl@ucf.edu

Ali P. Gordon
University of Central Florida
Orlando, FL, USA
apg@ucf.edu

ABSTRACT

Contemporary computing packages handle a wide variety of stress analysis types, but are yet to provide an optimal way to handle certain load cases and geometries. Blades in gas turbine systems, for instance, undergo repetitive thermal and mechanical load cycles of varied shape and phasing. Complexly-shaped airfoils create non-uniform stress paths that exacerbate the problem of FEA software attempting to determine the correct states of stress and strain at any point during the load history. This research chronicles the update and integration of Miller's original viscoplasticity model with ANSYS finite element analysis software. Elevated temperature strain-controlled LCF and strain-controlled TMF loadings were applied to single-element, uniaxial simulation runs and the results were then compared to data from duplicate experimental testing. Initial findings indicate that the model maintains significant accuracy through several cycles, but longer tests produce varying error in hysteretic response. A review of the modernized implementation of Miller's viscoplasticity model is presented with a focus on modifications that may be used to improve future results.

INTRODUCTION

Efficient gas turbine operation without the need for overly conservative service intervals is of paramount importance to the energy and aerospace industries. Thermomechanical Fatigue (TMF) -capable models are a core essential in creating accurate numerical simulations that ultimately can be used as a life-prediction tool for turbine components [1]. It has been theorized that contemporary computing packages can be used to augment viscoplasticity models that display a wide range of applicability. While it is not expected that such a constitutive model could properly predict times for fracture initiation or failure, it is reasoned that predictions of approximate stress/strain states in hardening, softening, or stable regions during the lifetime of a part are quite useful. The model selected for review in this study is the 1976 Miller viscoplasticity model, which has been demonstrated to be accurate in a variety of monotonic, cyclic, high-temperature, and creep loadings [2]. The commercial computing package ANSYS was utilized to supply loadings that simulate elevated temperature low cycle fatigue (LCF) as well as TMF to the model. While Miller's model does not explicitly support non-isothermal cases, ANSYS can supply the model updated temperature-dependent parameters when it passes the boundary conditions with each successive simulation step [3]. Although TMF loadings can incorporate many additional sub-mechanisms and interactions not present in LCF, [4-6] it is reasoned that simulations of the current level of sophistication can already meet an intermediary goal of providing accurate initial stress/strain responses and stress histories through the first 100 cycles of a load history.

In the present study, simulation data is gathered from both Miller's unaltered model and the ANSYS augmented model under elevated LCF and TMF conditions. These results are then compared with a mixture of historical and new experimental data from matching load conditions. It is shown that the ANSYS-adapted Miller model maintains a notable degree of accuracy for simulated fully-reversed cyclic loadings in steel with significant plasticity at elevated temperatures. However, examination of the hysteresis loops and stress histories beyond the region where initial work-hardening occurs reveals increasing error versus the experimental LCF cases.

For TMF load simulations, both in-phase (IP) and out-of-phase (OP) TMF cases with similar fully-reversed strain ranges initially match the stress and strain responses of some similar experimental data well [7]. Even so, successive cycling leads to error that increases versus the experimental data earlier in the load history than in the LCF case. A mismatch or misformulation of the parameters that govern the isotropic and

kinematic hardening behavior may constitute the driving mechanism behind the progressive error in both the TMF and LCF cases. The handling of the non-isothermal loads externally specifically seems to inadvertently induce an artificial kinematic hardening effect not observable in the LCF cases, as the yield surfaces can be observed to be translating with each successive cycle and increasing the peak stress errors asymmetrically.

NOMENCLATURE

σ	applied stress [MPa]
ε_{mech}	total mechanical strain [%]
ε	nonelastic strain [%]
R	rest stress [MPa]
D	characteristic drag stress [MPa]
A_1, A_2, B, C_2	material model behavioral constants
H_1, H_2	hardening behavior constants
Q	plastic flow activation energy [kJ/mol]
n	loss/recovery exponent
θ'	temperature dependency factor

MATERIAL

Type 304 stainless steel was an ideal candidate for this particular study for three primary reasons: Firstly, this grade of austenitic steel is widely used in a number of industries under a variety of conditions. These include high temperature isothermal and thermomechanical fatigue cycling in energy and petrochemical applications. Secondly, the foundations of the Miller viscoplasticity model were developed with this specific alloy, so it can be expected that the behavioral constants for the material as well as the model response should be optimal. Additionally, the relative low cost and machinability of 304 SS increases the feasibility of a more comprehensive experimental scheme.

Historically, 304 SS is already documented to have a number of desirable properties for energy applications [8, 9]. Basic material behavior and isothermal strain-life data for temperatures up to and exceeding 800°C is widely available in literature [10-13]. Although lacking the toughness and oxidation resistance of nickel-based alloys, high chromium content ensures above average defense against oxidation, while significant strength is retained at such elevated temperatures [14]. Type 304 SS microstructure is dominated by large austenite grains that are outlined by darker carbide-heavy boundaries. Chemical composition is available in Table 1.

Table 1: Alloying Agent Composition [15]

Alloying agent	Symbol	% Composition
Chromium	Cr	18.0-20.0
Nickel	Ni	8.0-10.5
Manganese	Mn	2.00
Silicon	Si	1.00
Carbon	C	0.04-0.10
Phosphorus	P	0.045
Sulfur	S	0.030

Sensitization is known to occur with long-term application of heat, evidenced by growth of the brittle carbide deposits [15] that are found at the grain boundaries. Additionally, the large austenite grains are significantly lengthened in worked 304 SS, leading to large increases in tensile strength with some conditioning practices. All 304 SS specimens utilized in this study were machined from annealed, as-wrought material.

SPECIMEN CONFIGURATION AND TESTING

New experimental data for the study was gathered during mechanical testing of smooth, round, dogbone-shaped fatigue samples, with relevant specimen geometry given as shown in Fig. 1.

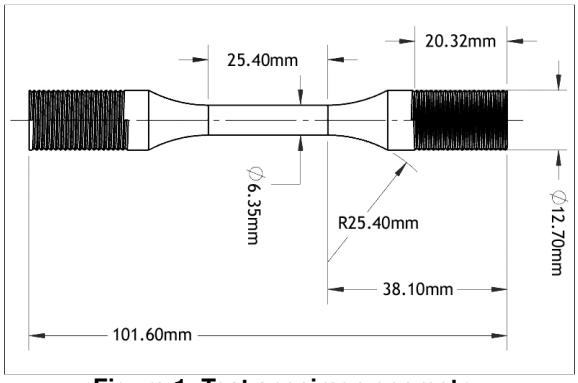

Figure 1: Test specimen geometry

A 100-kN MTS servohydraulic testing frame was utilized in conjunction with an Ameritherm HOTShot 3500W induction heating system to apply the requisite mechanical and thermal loads for the elevated LCF and TMF test types examined in the study. A general view of the experimental apparatus is shown in Fig. 2.

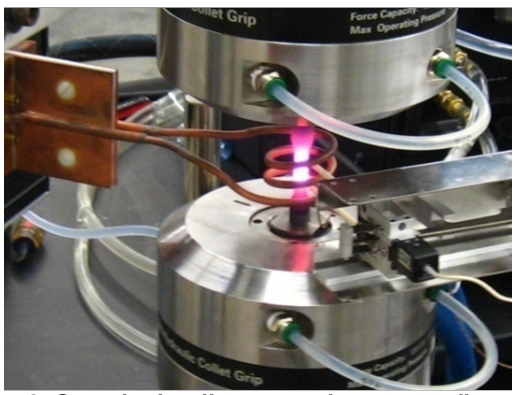

Figure 2: Servohydraulic test equipment configuration

Fully-reversed elevated temperature LCF tests were conducted in accordance with ASTM standard E606 [16] at 600°C with a mechanical strain range of 0.7%, and a strain rate of 6% per minute. Specimens under these conditions exhibited

noticeable isotropic hardening initially, followed by a period of softening lasting several hundred cycles before stress stabilization occurred.

Thermomechanical fatigue tests were also conducted as fully reversed, with a mechanical strain range of 0.7% in both in-phase and out-of-phase configurations. In each case, a minimum temperature of 200°C and a maximum temperature of 600°C were applied. TMF tests were conducted in accordance with ASTM standard E2368 [17]. A mechanical strain rate of 0.84%/min and a matching thermal rate of 240°C/min were employed in both IP and OP TMF tests. Specimens subjected to these thermomechanical fatigue conditions also experienced initial hardening, followed by softening and stress stabilization – albeit with overall lifetimes reduced significantly. A summary of experimental data sources employed in this experimental and numerical comparative analysis are available in Table 2.

Table 2: Experimental load cases

Load Case	Strain Ratio, R_ε	Mech. Strain Range, $\Delta\varepsilon_{mech}$	Max Temp, T_{max}	Min Temp, T_{min}	Data Source
LCF	-1	1.0%	593C	593C	Miller/Corum
LCF	-1	0.7%	600C	600C	UCF
IP TMF	-1	0.7%	200C	600C	UCF
OP TMF	-1	0.7%	200C	600C	UCF

NUMERICAL MODEL ADAPTATION

Miller's original viscoplasticity model has been adapted to the commercial computation package ANSYS as a user programmable feature (UPF) for use in the current study. A Fortran 90 subroutine was implemented as a user plasticity law governed directly by the principal formulation of Miller's model, given as follows:

$$\dot{\varepsilon} = B\theta' \left\{ sinh\left[\left(\frac{|\sigma - R|}{D} \right)^{1.5} \right] \right\}^n sgn\,(\sigma - R) \qquad (1)$$

Additionally, the subroutine also calculates a version of the characteristic drag stress, D, and the rest stress (also commonly known as back stress), R, per execution step. Miller's expressions for drag stress and back stress directly control isotropic hardening and kinematic hardening behaviors of the model [18], respectively. The model calculates the changes in these values per time step, and the expressions are given by the following equations:

$$\dot{R} = H_1\dot{\varepsilon} - H_1 B\theta' [sinh(A_1|R|)]^n sgn\,(R) \qquad (2)$$

$$\dot{D} = H_2|\dot{\varepsilon}| \left[C_2 + |R| - \left(\frac{A_2}{A_1} \right) D^3 \right] - H_2 C_2 B\theta' [sinh(A_2 D^3)]^n \qquad (3)$$

During execution, material constants, behavioral constants, and boundary conditions for the solution step are handled externally by the inbuilt ANSYS code. Stress/strain states that induce plasticity transfer relevant quantities to the subroutine. Historical changes in the model response are implemented through continual updates of the resultant R and D values as state variables.

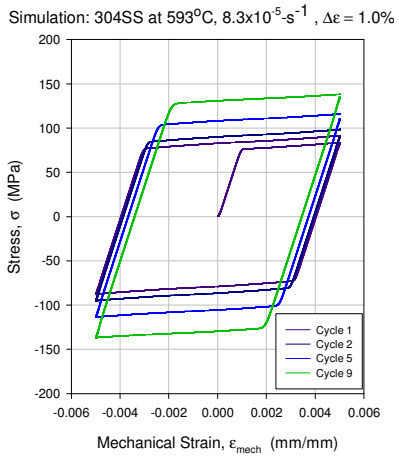

Figure 3: Simulated strain-controlled LCF at 593°C

Illustrated in Figure 3, the response of the modernized implementation closely matches that of the original MATMOD simulations.

HIGH TEMPERATURE FATIGUE RESULTS

Comparison of the model's stress response for high temperature LCF with that of data used by Miller from Corum [19] reveals a reasonable qualitative fit, with decreasing isotropic hardening being the primary dynamic feature of the cyclic stress/strain response. Minimum error occurs at the peak and valley stresses for each cycle, with the model initially greatly overestimating these values.

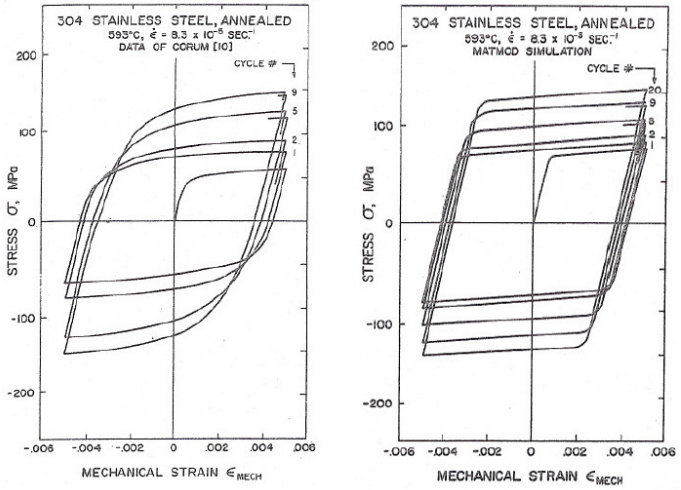

Figure 4: Comparison of 304SS LCF loading [from 2]

Between cycles 5 and 9, hardening effects become less severe, and the model begins consistently underestimating the peak values by between 10% and 15%. Analysis of the stress history of the model through 100 cycles shows that decreasing hardening occurs on the way to permanent stabilization in several tens of load reversals.

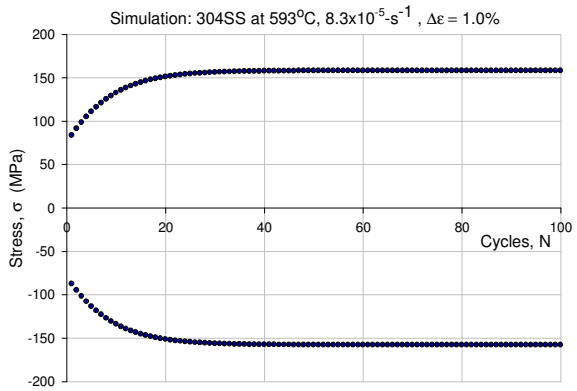

Figure 5: Stress response of original model to 100cycles

Assessment of the model versus the UCF data in the 0.7% strain range case infers additional behavioral differences. While the model shows similar isotropic hardening over several tens of cycles before permanent stabilization, this effect gives way to continual softening after the first few cycles in experimental testing. Additionally, the Miller model is extremely under-conservative in its estimate of stress response throughout the history.

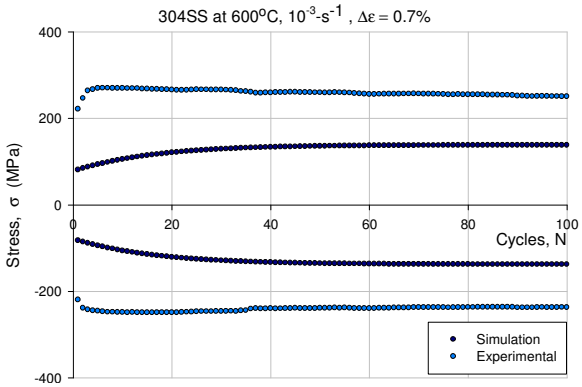

Figure 6: Stress history comparison for 600°C LCF

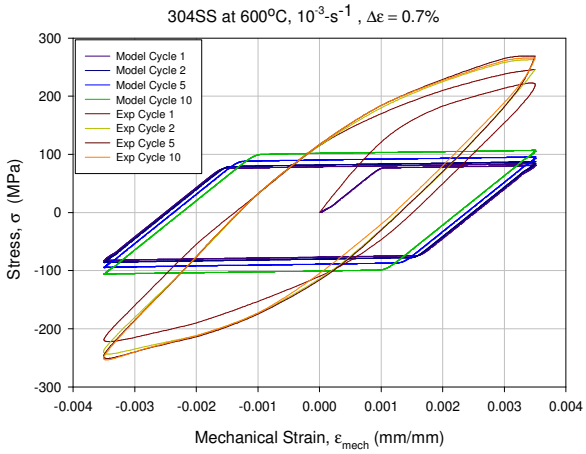

Figure 7: Cycle comparison for 600°C LCF

THERMOMECHANICAL FATIGUE RESULTS

In relation to the Miller model predictions versus the LCF cases, both IP and OP TMF cases exhibited more favorable correlations with the experimental data. For the in-phase instance the model correctly predicts that substantial hardening will occur within the first cycle, and is in agreement with the experimental data regarding the minimum stresses per cycle.

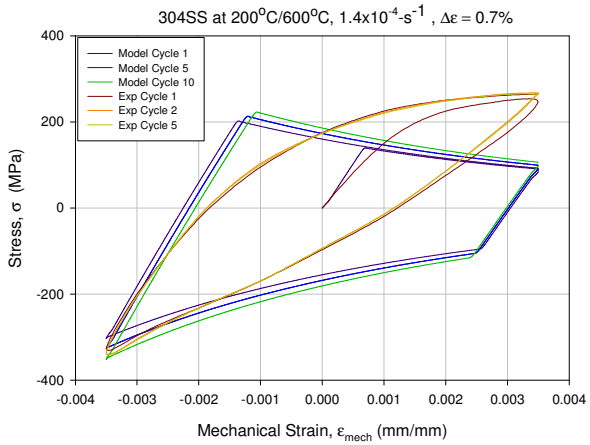

Figure 8: Comparison of cyclic response- IP TMF case

As with the LCF cases, the model predicts continually decreasing isotropic hardening before stabilizing within 100 cycles- however, the tested specimens tend to exhibit softening after the first 5 to 10 cycles.

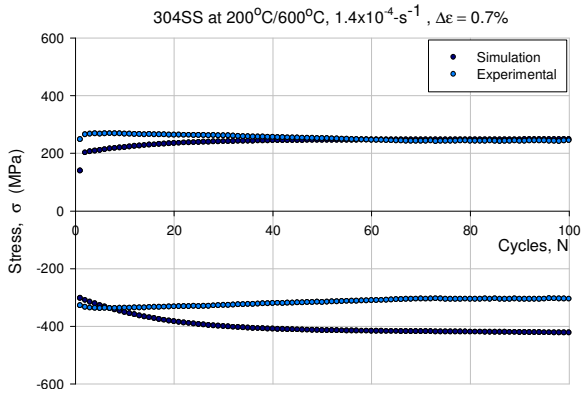

Figure 9: IP TMF Stress history comparison

This opposition of behaviors leads to the simulation and experimental stress peaks eventually converging, while the minimum stresses per cycle settle at near 25% error.

In the OP simulation run, the Miller model accurately predicted that the hardening in the initial cycles was less intensive than in other cases. Additionally, inspection of the stress histories reveals that the OP case shows the only noticeable evidence of kinematic hardening, occurring in the first few cycles- during this period, the Miller simulation shows asymmetric hardening response favoring the direction of the kinematic hardening.

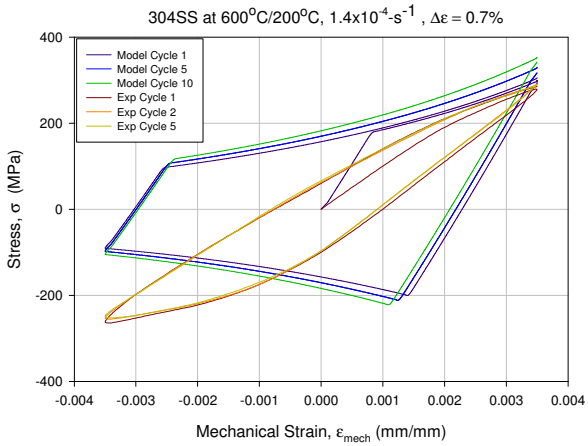

Figure 10: Comparison of cyclic response- OP TMF case

Stress minimums per cycle match closely with those of the experimental data, but as with previous cases do not occur at the same strain level. After stabilization, stress maximums are overly conservative by levels exceeding 30%.

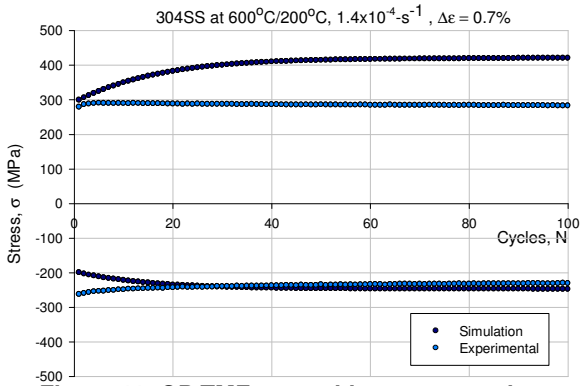

Figure 11: OP TMF stress history comparison

DISCUSSION

In general, the reviewed model has a mixture of favorable features and shortcomings when compared with real-world behavior of type 304 stainless steel. The formulations that govern the stresses *R* and *D* provide kinematic and isotropic hardening effects to both LCF and TMF cases with levels of intensity proportionally appropriate. In the broader sense of adapting the model to non-isothermal cases, the Miller model and its handling (or lack thereof) of direct temperature dependencies was not an issue with ANSYS correctly mediating the ongoing boundary condition changes. Additionally, TMF load cases infer a slower mechanical strain rate versus LCF, and the difference in the UCF data was an order of magnitude in this case. Poor correlation between simulations and the UCF isothermal data yet better observed correlation with the TMF data is indicative of a strain rate dependency that directly affects accuracy. Simulation response of LCF at 593°C properly correlates with the historical data, but hardly differs from the response of the 600°C cases with a higher strain rate. The simulation of higher strain rate LCF cases, of course, showed wide variation from the experimental response. Though mentioned in the follow-up to the original Miller paper, this strain rate sensitivity may prove to be less moderate than previously anticipated.

In order for this particular viscoplasticity model to be useful in life prediction methodologies, increased accuracy in the stress/strain states encountered well beyond the first few cycles will be necessary. Though Miller's original model was initially designed to handle materials that show significant work hardening, there appears to be insufficient ability to handle eventual reversal of hardening effects. The model itself is capable of this behavior with slowly decreasing drag stress, but it seems that the values passed from state to state are very small compared to what is necessary to impact the overall behavior. This presents a considerable shortcoming in regard to accuracy in later cycles, especially for loadings with a high degree of plasticity that are expected to weaken and fail quickly. For every case examined during this study, hardening became qualitatively negative after only a few cycles in the test specimens, but continued on indefinitely in simulation.

Inspection of individual simulation cycles indicates general agreement with experiments in terms of hysteretic energy and stress states accompanying strain end levels. It is clear however, that the yield surface shapes differ greatly. The propensity of the simulation software to separate behavior into clear elastic and plastic regimes causes appreciable differences in response when appropriate levels of plasticity are not encountered in the load condition.

MODEL UPDATES AND MODIFICATIONS

More recent iterations of Miller's model have enhanced the base accuracy of the method through several fundamental reformulations. Handling of dynamic aging effects, along with the use of several competing hardening/recovery factors is shown to improve the isotropic hardening response. The back-stress term is augmented with an additional recovery term which helps the kinematic response behave in a less linear and a simplistic manner. Previously independent back-stress and drag stress terms are coupled together, with the drag stress including a secondary coupling to the total strain rate [20]. While this type of structuring might allow for more direct handling of the strain rate issues encountered in this study, the most recent formulation does not yet alleviate the problem.

Rudimentary modification of the model to suit specific needs could be accomplished through a few types of simplistic changes. Firstly, it appears to be feasible through the adjustment of the behavioral constants to reflect a focus on specific regimes. For instance, the scaling of just the H_1 and H_2 constants can be changed to values that significantly decrease the error when considering the higher strain rate UCF data. Another approach involves addition of a damage or weakening function that is heavily dependent on model memory, thusly providing a mechanism for eventual softening without the necessity of directly addressing the issue of a saturated drag stress. These methods, though workable, are not preferred to a more accurate parent model.

REMARKS AND RECOMMENDATIONS

In its present state of development, the Miller viscoplasticity model does not provide a tool for reliable determination of late TMF cycle stress/strain states. Even so, the present incarnation does serve as the basis for an adaptable constitutive model. Remarks about the study and further improvements that should be considered are as follows:

1) It must be noted that adaptation of the original model to ANSYS produced subtle variations in the LCF solutions when compared to the original MATMOD runs. An investigation of ANSYS versus MATMOD variable precision and solving methods may yield insight into the differences.

2) Though the Miller model does not explicitly incorporate a yield stress, it is clear that the handling code in ANSYS (and historically in MATMOD) separates the solution into simple elastic and Miller-calculated plastic regimes. In order for the yield surfaces of the model to more accurately mimic their real-life counterparts, a method which facilitates a smooth transition in simulation behavior is desired. Future iterations of development may want to attempt to incorporate a competitive parallel calculation of elastic and plastic components, or utilize a Ramberg-Osgood type of curve fit to relevant parts of the hysteresic response.

3) Especially for materials that easily and significantly display initial work hardening behavior, it seems that an explicit handling of negative hardening effects may be necessary. The current handling of the drag stress allows for this in the model, so an updated version of Equation 3 that includes a more dominant time- or cycle-dependent term may be worth consideration.

4) In non-isothermal cases, a variety of different effects occur that significantly impact the stress/strain states and cyclic lifetimes. Damage and recovery due to a wide array of mechanisms can occur with varying interaction and synergy amongst one another [21]. It is unlikely that a specific fit of TMF behavior is attainable through many cycles unless additional behavioral complexity is incorporated via functions and material constants determined by TMF testing [22].

5) Currently, the model displays unacceptable levels of error, yet is still quite mathematically convoluted. At present, expansion of the model to multi-element or multiaxial cases should be reserved for when the previously mentioned issues are met with resolution.

ACKNOWLEDGMENTS

The authors of this paper would like to thank members Francis J. Tam, Calvin M. Stewart, and Scott G. Keller of the University of Central Florida's Mechanics of Materials Research Group for assistance with this study.

REFERENCES

1. Gordon, A. P., Williams, E. P., and Schulist, M., "Applicability of Neuber's Rule to Thermomechanical Fatigue," *Proceedings of ASME Turbo Expo*, 2008.
2. Miller, A., "Inelastic Constitutive Model for Monotonic, Cyclic, and Creep Deformation: Part II- Application to Type 304 Stainless Steel," *Journal of Engineering Materials Technology.* Vol. 98H(2), pp. 106-1112, 1976.
3. ANSYS, Inc., 2006. *Guide to ANSYS User Programmable Features*, ANSYS Corporation, Canonsburg, PA.
4. Taira, S., "Relationship between Thermal Fatigue and Low-Cycle Fatigue at Elevated Temperature," *Fatigue at Elevated Temperatures*, ASTM STP 520, pp. 80-101, 1973.
5. Taira, S., Fujino, M., and Ohtani, R., "Collaborative Study on Thermal Fatigue of Properties of High Temperature Alloys in Japan," *Fatigue of Engineering Materials and Structures.* Vol. 1, pp. 495-508, 1979.
6. Taira, S., Fujino, M., and Marayuma, S., 1974."Effects of Temperature and the Phase between Temperature and Strain on Crack Propagation in a Low Carbon Steel during Thermal Fatigue," *Mechanical Behavior of Materials,* Society of Materials Science, Kyoto.
7. Karl, J., "Thermomechanical Fatigue Life Prediction of Notched 304 Stainless Steel," Dissertation Prospectus, University of Central Florida, 2011.
8. Kuwabara, K., and Nitta, A., "Effect of Strain Hold Time of High Temperature on Thermal Fatigue of Type 304 Stainless Steel," *Proceedings of the ASME-MPC Symposium on Creep-Fatigue Interaction*, 1976.
9. Kuwabara, K., and Nitta, A., "Thermal-Mechanical Low Cycle Fatigue under Creep-Fatigue Interaction on Type 304 Stainless Steels," *Fatigue and Fracture of Engineering Materials and Structures.* Vol. 2, pp. 293-304, 1979.
10. Keisler, J. M., Chopra, O. K., Shack, W. J., "Statistical Models for Estimating Fatigue Strain-Life Behavior of Pressure Boundary Materials in Light Water Reactor Environments," *Nuclear Engineering and Design*. Vol. 167, pp 129-154, 1996.
11. Colin, J., Fatemi, A., Taheri, S., "Fatigue Behavior of Stainless Steel 304L Including Strain Hardening, Prestraining, and Mean Stress Effects," *Journal of Engineering Materials and Technology*. Vol. 132, pp. 08-13, 2010.

12. Solomon, H. D., Amzallag, C., DeLair, R. E., and Vallee, A. J., "Comparison of the Fatigue Life of Type 304L SS as Measured in Load and Strain Controlled Tests," *Proceedings of the 12th International Conference on Environmental Degradation of Materials in Nuclear Power System Water Reactors*, 2005.
13. Coffin, L. F., 1979. "Fatigue in Machines and Structures – Power Generation," *Fatigue and Microstructure*, Meshii, M., Editor, ASM International, Metals Park, OH.
14. Ashby, M. F., 2005. *Materials Selection in Mechanical Design, Third Edition*, Elsevier Butterworth-Heinemann, Oxford, UK.
15. Lampman, S. and Zorc, T., Editors, 2007. *ASM Handbook-Properties and Selection: Irons, Steels, and High-Performance Alloys*, ASM International, Metals Park, OH.
16. E-606, 2004. *Standard Practice for Strain-Controlled Fatigue Testing,* ASTM International, West Conshocken, PA.
17. E-2368, 2004. *Standard Practice for Strain-Controlled Thermomechanical Fatigue Testing*, ASTM International, West Conshocken, PA.
18. Miller, A., "Inelastic Constitutive Model for Monotonic, Cyclic, and Creep Deformation: Part I- Equations Development and Analytical Procedures," *Journal of Engineering Materials Technology.* Vol. 98H(2), pp. 97-105, 1976.
19. Corum, J. M., "Material Property Data for Elastic-Plastic-Creep Analyses of Stiffened Shear-Lag Panel," Appendix C to report #ORNL-SUB-3754-1, by R. L. Egger, p. 222, 1974.
20. Chaboche, J.L., "A Review of Some Plasticity and Viscoplasticity Constitutive Theories," *International Journal of Plasticity.* Vol. 24, pp. 1642-1693, 2008.
21. Fujino, M., and Taira, S., "Effect of Thermal Cycling of Low Cycle Fatigue Life of Steels and Grain Boundary Sliding Characteristics," *Proceedings of the International Conference on Mechanics 3*, 1979.
22. Sehitoglu, H., 2006. "Overview of High Temperature and Thermo-Mechanical Fatigue (TMF)," Presentation given at University of Illinois Urbana-Champaign, Urbana, Ill.